



Performance Improvement of Ultrathin CIGS Solar Cells Using Al Plasmonic Nanoparticles: The Effect of the Position of Nanoparticles

Sahar Royanian¹, Ali Abdolhazadeh Ziabari^{*,2}, Reza Yousefi¹, Seyed Saleh Ghoreishi¹

¹ Department of Electrical Engineering, Nour Branch, Islamic Azad University, Nour, Iran

² Nano Research Lab, Lahijan Branch, Islamic Azad University, Lahijan, Iran

(Received 13 Sep. 2020; Revised 21 Oct. 2020; Accepted 14 Nov. 2020; Published 15 Dec. 2020)

Abstract: CIGS solar cells are regarded to be one of the best thin film solar cells with efficiencies up to 22.6%, which exceeds the current multicrystalline Si record efficiency (21.9%). To make the promising CIGS solar cells more economic, reduction of costly In and Ga elements through thinning of CIGS layer seems necessary. But, it causes the cell performance degradation. This study is aimed to investigate the efficiency enhancement of ultrathin CIGS solar cells by using of Al plasmonic nanoparticles. Plasmonic nanoparticles can restrict, absorb, navigate or scatter the incident light. The role of different location of Al nanoparticles within the active layer was studied through optical and electrical simulation utilizing FDTD and DEVICE solvers of Lumerical software. By using the spherical Au nanoparticles, the light absorption in the cell increased drastically. The highest $\eta=15.31\%$ was achieved for the designed ultrathin CIGS solar cell decorated by Al nanoparticles located in the middle of the absorber layer.

Keywords: Al Nanoparticles, CIGS, FDTD, Light Trapping, Surface Plasmon

1. INTRODUCTION

Photovoltaic (PV) solar cells are optoelectronic devices that absorb the sunlight and convert it to electricity [1-5]. Because of environmental and geopolitical challenges, there are lots of attentions into the use of unlimited and clean solar energy [6-10]. However, there is still a long way to go for generalization of PV solar energy. In comparison to the costly crystalline silicon solar cells, thin film solar cells (TFSCs) show moderate efficiencies and much lower fabrication cost [11-18]. As one of the most promising TFSCs, copper indium gallium selenide (CIGS) solar cells have shown superior properties.

* Corresponding Author. Email: ali.abd.ziabari@gmail.com , ali_abdolhazadeh@liau.ac.ir

CIGS is composed of CInSe_2 and CGaSe_2 that results in a quaternary compound with properties common between both components. Commonly, the conventional thickness for CIGS layer in TFSCs, is 2–3 μm that seems noneconomic because of the presence of expensive In and Ga elements [19]. Hence, thinning the absorber layer seems inevitable to fabricate economic solar cells by saving on raw materials and reducing the production time and energy. However, as the thickness of the absorber layer decreases the number of the absorbed photons also decreases. Thus, the efficiency of the solar cell decreases remarkably. Using plasmonic nanoparticles (PNPs) can help to absorb more incident photons. PNPs with appropriate shape, period and location can enhance the optical path length inside the solar cells, thus increasing the light trapping and the efficiency of the solar cell. This occurs because of increase in the light absorption by excitation of localized surface plasmons (LSPs). Reports on PNPs embedded in CIGS solar cells are very rare. In our previous study [20], the influence of size and period of spherical Au NPs loaded on the topmost layer of ultrathin CIGS solar cell was investigated. In the present study, the effect of embedment of Al NPs in different vertical locations inside the active layer is analysed. To our knowledge, reports on this issue for ultrathin CIGS solar cells are rare. Generally, the vertical location of PNPs determines whether the light scattering into the cell causes the absorption enhancement or the near field effect. Ghahremanirad et al [21] have investigated the influence of the location of the embedded Au NPs on the optical absorption of perovskite solar cells. Results revealed that Au NPs embedded in the middle of the absorber layer could enhance the light absorption more than the other locations. Al NPs were used in this study because of: relatively strong surface plasmon resonance (SPR) response compare to other metals and much lower price than Au.

2. METHODOLOGY

A method including three steps is pursued in this work: a) verification of the simulation process, b) applying the planned modifications and c) optimization of the designed structure. Fig.1a shows the structure of a conventional CIGS solar cell while Figs.1b–d display the CIGS solar cells decorated by spherical Al NPs located at up, middle and down of the active layer. The NPs with diameter D have been arranged in an array with a period of P . The stacking order of different layers from back contact to window layer is as $\text{Mo/CIGS/CdS/ZnO/ITO}$. Generally, a MoS_x layer is formed at the Mo/CIGS interface because of the reaction between CIGS and Mo during fabrication process. The finite-difference time-domain (FDTD) technique is used in this study to investigate the light propagation in the solar cell. Using Maxwell's time-domain curl equations, FDTD results in the electrical and magnetic fields components (i.e. E_x , E_y , E_z , H_x , H_y and H_z). The derivatives in the curl equations are calculated by a finite-difference approximation on a mesh grid. FDTD

calculates the field components at every grid point for every time step. The FDTD and DEVICE simulators of Lumerical software were applied to calculate the optical and electrical characteristics of the modeled solar cells [22,23]. Aluminum nanoparticles area was meshed by mesh units of $1\text{nm}\times 1\text{nm}$ for high precision. The periodic boundary conditions (PBC) were applied at lateral boundaries of the modelled device to keep the uniform periodicity of the NPs.

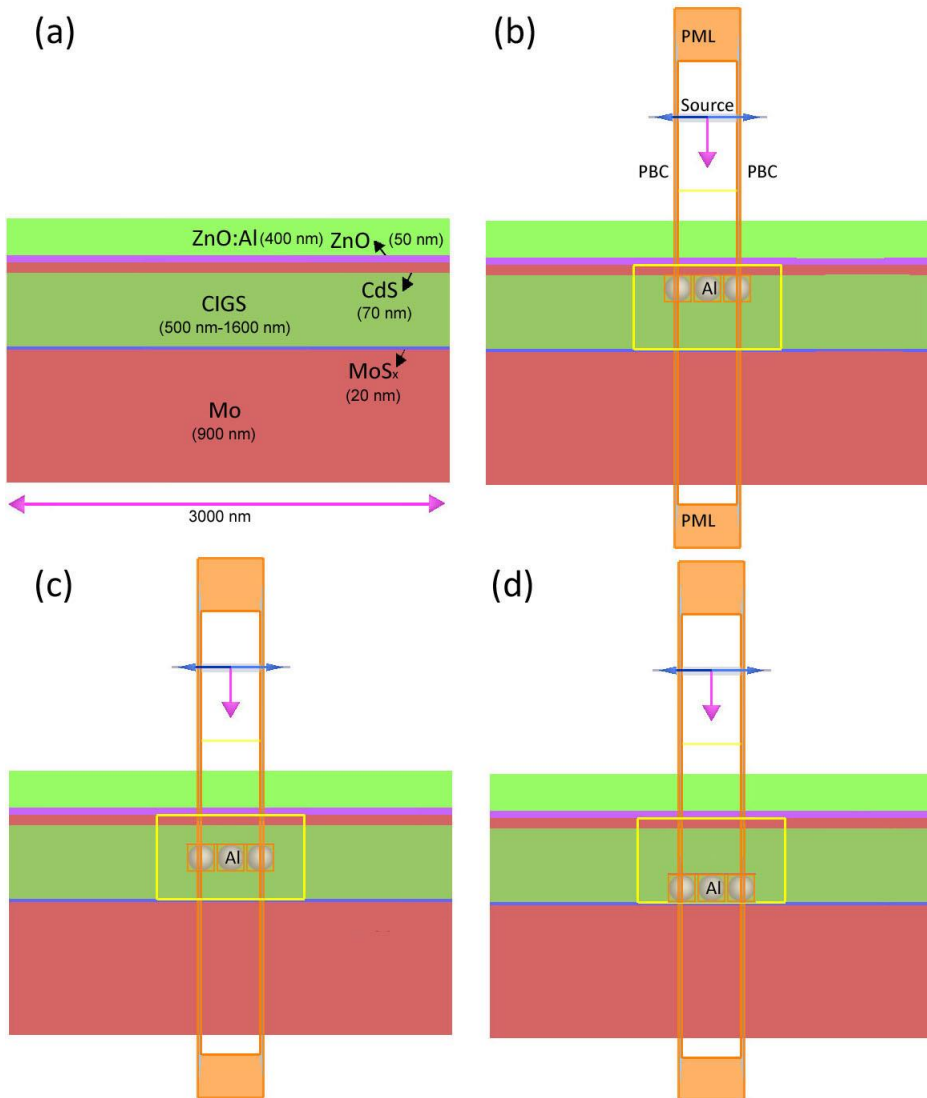


Fig. 1. Schematic of the modelled CIGS solar cell: (a) without NPs or bare cell, with spherical Al NPs located at (b) up, (c) middle and (d) down of the absorber layer.

Al nanoparticles area was meshed by mesh units of $1\text{nm}\times 1\text{nm}$ for high precision. The periodic boundary conditions (PBC) were applied at lateral boundaries of the modelled device to keep the uniform periodicity of the NPs. Besides, the perfectly matched layer (PML) boundary conditions were utilized in the incident direction to hinder any interference effect. To define the optical properties of the materials in FDTD the related complex refractive index was used [24]. The data for CIGS compound were extracted from a recently published experimental report [25]. The simulation was carried out using the physical parameters of the materials stored in Lumerical library. The modelled solar cells were irradiated with AM1.5G spectra. The outputs of the absorbed power and generation rate were then used in an electrical simulation which solves the Poisson and drift–diffusion equations in DEVICE solver. Finally, the calculated optical and electrical properties were used to calculate the PCE of the solar cells.

3. Results and discussion

3.1. Verification of simulation

The study was started with simulation of a reference cell [25] (Fig. 1a) to validate the accuracy of the procedure. The simulated and experimental J–V curves have been shown in Fig. 2. The qualitative output values including the short–current density (J_{sc}), open circuit voltage (V_{oc}), fill factor (FF) and power conversion efficiency (PCE or η) have been shown inside the figure. As it is evident, the calculated and simulated data are in a quite good agreement with each other. This verifies the validity of the calculation process.

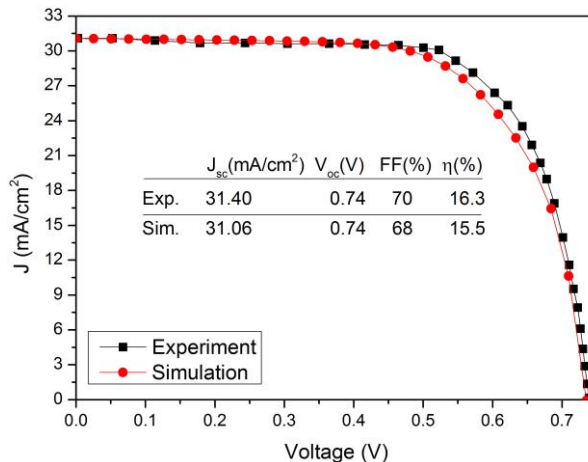


Fig. 2. J–V curves for the reference CIGS solar cell along with the pertinent simulated solar cell [25].

3.2. The effects of CIGS layer thicknesses on the cell performance

Fig. 3 indicates the variation of (a) absorption, (b) J–V characteristic and (c) external quantum efficiency (EQE) of the modelled CIGS solar cell for three different values of the thickness of CIGS layer. The corresponding solar cell performance parameters have been listed in Table 1.

As the thickness of the active layer decreased the absorption and EQE of the solar cell decreased too especially beyond $\lambda=550$ nm. As a consequence, the short circuit current reduced due to decrease in the number of electron–hole pairs. This clearly shows the degradation of the performance of the solar cell by thinning of the active layer. On the other hand, from Fig. 3a, the highest absorption occurs around 800–900 nm corresponding to the band edge of CIGS layer. Remarkable fluctuations get started below this region and show strong ups and downs under 600 nm. These fluctuations are related to the fringes stemming from constructive/destructive interference between the beams coming out of different layers of the cell. Apparently, this is more obvious for the short wavelength waves.

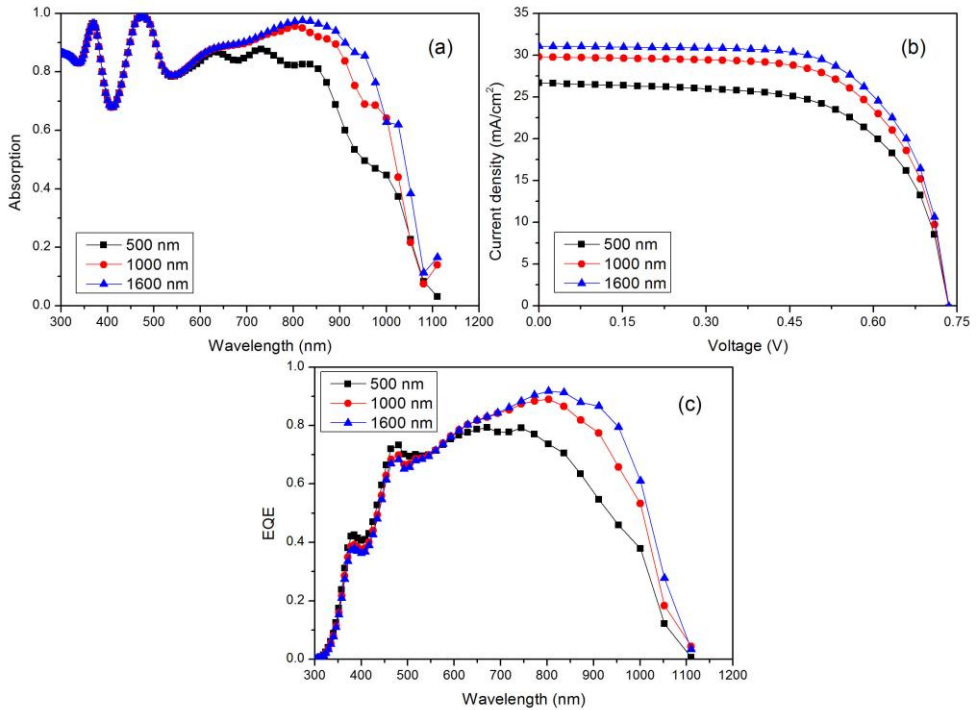


Fig. 3. (a) the absorption spectra, (b) J–V curves and (c) EQE of CIGS solar cells with different absorber layer thicknesses.

Table 1. Photovoltaic data of CIGS solar cell with different absorber layer thicknesses.

CIGS thickness	J_{sc} (mA/cm ²)	V_{oc} (v)	η (%)	FF (%)
1600 nm	31.06	0.740	15.50	67.45
1000 nm	29.78	0.739	14.59	66.33
500 nm	26.65	0.735	12.57	64.00

3.2. Using Al plasmonic nanoparticles

To improve the performance of the ultrathin CIGS solar cell with thickness of 500 nm, the Al PNPs are used. Embedment of Al NPs can lead to absorption enhancements in long wavelengths. Therefore, using Al NPs is expected to improve the performance of the ultrathin CIGS solar cell. PNPs can scatter the light strongly at wavelengths near to the plasmon resonance. The scattering and absorption cross-sections are given by [26]:

$$C_{Scat.} = \frac{1}{6\pi} \left(\frac{2\pi}{\lambda} \right)^4 |\alpha|^4 \quad (1)$$

$$C_{Abs.} = \frac{2\pi}{\lambda} \text{Im}(\alpha)$$

where

$$\alpha = 3V \left[\frac{\frac{\epsilon_p}{\epsilon_m} - 1}{\frac{\epsilon_p}{\epsilon_m} + 2} \right] \quad (2)$$

here α is the polarizability of PNPs, V is the PNPs volume, ϵ_p is the dielectric function of the PNPs and ϵ_m is the dielectric function of the surrounding material. PNPs polarizability will become very large when $\epsilon_p = -2\epsilon_m$. This takes place when the frequency is close to the surface plasmon resonance (SPR) ω_{sp} , thus the light interacts over an area larger than the geometric cross section of the particle. Dielectric function of metals can be described by the well-known Drude model [26]:

$$\epsilon = 1 - \frac{\omega_p^2}{\omega^2 + i\gamma\omega} \quad (3)$$

where ω_p is the bulk plasmon frequency given by $\omega_p = \sqrt{Ne^2/m\epsilon_0}$, where N is the density of free electrons, m is the effective mass of an electron, e is the electronic charge and ϵ_0 is the free-space dielectric constant. From Eqs. 2 and 3, one can easily obtain

$$\alpha = 3V \frac{\omega_p^2}{\omega_p^2 - 3\omega^2 - i\omega\gamma} \quad (4)$$

Therefore, the SPR frequency for a sphere in free space happens at $\omega_{sp} = \frac{1}{\sqrt{3}} \omega_p$ and basically depends on the density of free electrons in the

particle. The PNPs improve the light absorption in the semiconductor depending on their localization by three mechanisms. Firstly, PNPs can be placed on the top surface of a solar cell where light can get scattered at different angles to increase the path length in the absorber layer. Secondly, they can be embedded into the semiconductor to get localized surface plasmonic (LSP) enhancement by increasing the optical absorption especially close to the metal surface plasmons which increase light intensity and therefore an increase in optical

absorption. Third, they can be located at the bottom of the active layer. In this case, photonic wave guiding modes or even surface plasmon polariton (SPP) modes can be formed which would propagate parallel to the surface of the metal and there would be a decaying field into the semiconductor. The optical properties of nanoparticles depend strongly on the size, radius, material and the distance between them.

3.2.1. The effect of the radius and period of Al PNPs on the absorption of the solar cell

In this section, the aim is to find the optimum radius of Al NPs embedded at the top of CIGS layer (Fig. 1b). To investigate the variation of the solar cell efficiency with and without Al NPs, the integrated absorption factor G are defined as follows [27]

$$G(\lambda) = \frac{IQE_{PNPs}}{IQE_{Bare}} = \frac{\int \lambda P_{PNPs}(\lambda) I_{AM1.5}(\lambda) d\lambda}{\int \lambda P_{Bare}(\lambda) I_{AM1.5}(\lambda) d\lambda} \quad (5)$$

where IQE_{PNPs} and IQE_{Bare} are the integrated quantum efficiency (IQE) for the solar cell with and without PNPs (bare cell), respectively. Also, P_{PNPs} and P_{Bare} explain the power of the absorbed light in the presence of PNPs and without PNPs, respectively. Fig. 4a shows the integrated absorption factor G for different radii of Al NPs ranging from 30nm–120nm. As seen, the Al NPs radius has a great effect on the absorption enhancement factor of the solar cell. The highest value of G was achieved for diameter of 100 nm. The absorption enhancement parameter $g(\lambda)$, defines the ratio of quantum efficiency with PNPs to the quantum efficiency without PNPs

$$g(\lambda) = \frac{QE_{PNPs}}{QE_{Bare}} = \frac{P_{PNPs}(\lambda)}{P_{Bare}(\lambda)} \quad (6)$$

In Fig. 4b, the absorption enhancement parameters have been plotted as a function of wavelength. The highest value of about 1.38 was achieved for $D=100$ nm around $\lambda=425$ nm.

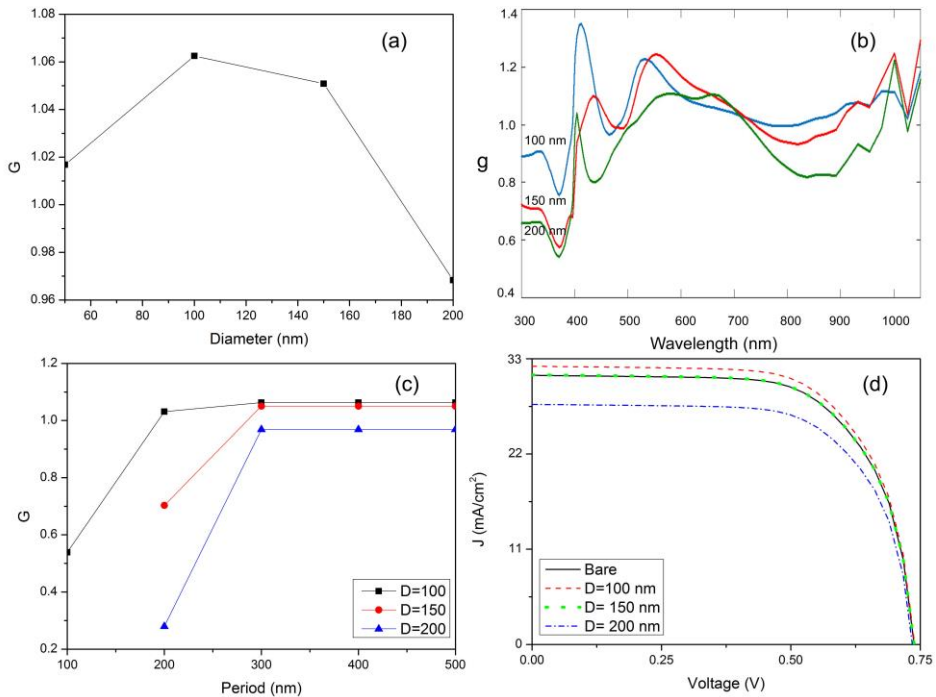


Fig. 4. Variation of (a) G factor as a function of Al PNPs, (b) enhancement parameter g versus wavelength, (c) G factor as a function of Al PNPs array period and (d) J-V characteristics of ultrathin CIGS solar cells decorated with Al NPs at different diameters.

The effect of the period of Al NPs array on the performance of the ultrathin CIGS solar cell at different diameter of NPs was also investigated. The results have been shown in Fig. 4c, where the integrated absorption factor G has been plotted versus period for different diameters of NPs. As the period distance between two NPs is increased, the absorption increased for all diameters and reached the maximum value at $P=300$ nm. As it is evident from the figure, NPs with $D=100$ nm and $P=300$ nm can enhance more effectively the light absorption in the solar cell. Taking $P=300$ nm, the J-V characteristic curves were plotted for different diameters of Al NPs. While the V_{oc} remained constant, the J_{sc} showed a notable variation with diameter of Al NPs and the optimum result was obtained for $D=100$ nm. Hence, Al NPs with $D=100$ nm arranged in an array with $P=300$ nm were opted for the next step of simulation.

3.2.2. The effect of the vertical position of Al NPs on the cell performance

One important parameter that remarkably affects the light absorption in a plasmonic solar cell is the location of PNPs. Therefore, the optimum

configuration obtained in the previous section, is investigated when the location of Al NPs varies in three different vertical positions, namely at the top, middle and bottom of ultrathin CIGS layer (Fig. 1b-d). Fig. 5 shows the calculated absorption spectra of the solar cell for three different vertical positions of Al NPs in comparison with the bare cell. Clearly, the embedment of Al PNPs in the bottom and the middle of the absorber layer increased the light absorption over a wide range of spectrum. Furthermore, for Al NPs embedded in the top of CIGS solar cell, the absorption is decreased in the range of 700–900 nm that may be related to the destructive interference between the scattered and incident light [20]. The calculated EQE spectra for the cells with three different locations of the PNPs have been shown in Fig. 6 alongside with the EQEs of the bare cell. Significant enhancement in EQE is observed in a broad wavelength range from 600 nm to 1100 nm for three different locations of PNPs nm compared to the bare cell. The enhancement observed here is greater than that was reported in the literature [28-30].

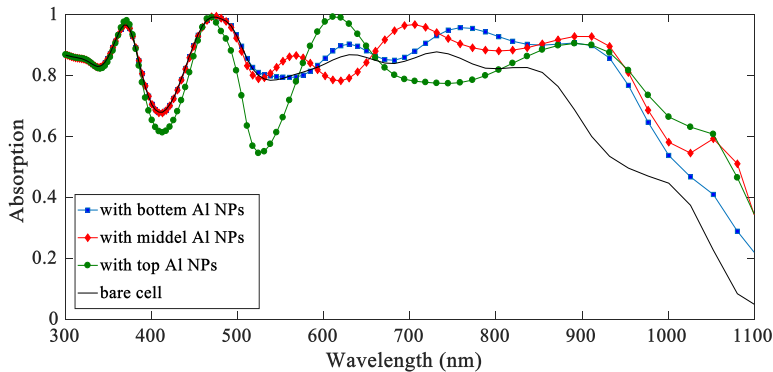


Fig. 5. Absorption spectra for ultrathin CIGS solar cells decorated with Al NPs at different vertical positions.

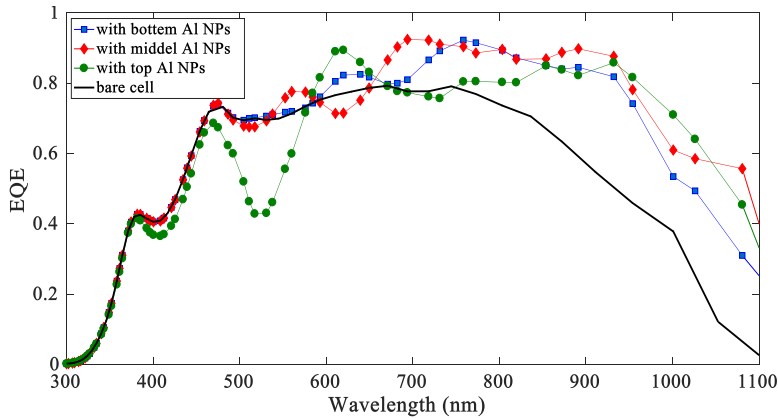


Fig. 6. The calculated EQE of ultrathin CIGS solar cell with three different locations of Al PNPs in comparison with the bare cell.

Fig. 7 exhibits the calculated corresponding J–V characteristics. Meanwhile, the solar cell parameters are listed in Table 2. It is observed that the FF decreased when the vertical position of Al NPs in CIGS layer changed from top to bottoms while the corresponding V_{oc} showed no change. The highest J_{sc} achieved when the Al NPs were located at the middle of the absorber layer. Also, the middle vertical position has the best efficiency of 15.31% with a J_{sc} of $32.03 \text{ mA}\cdot\text{cm}^{-2}$.

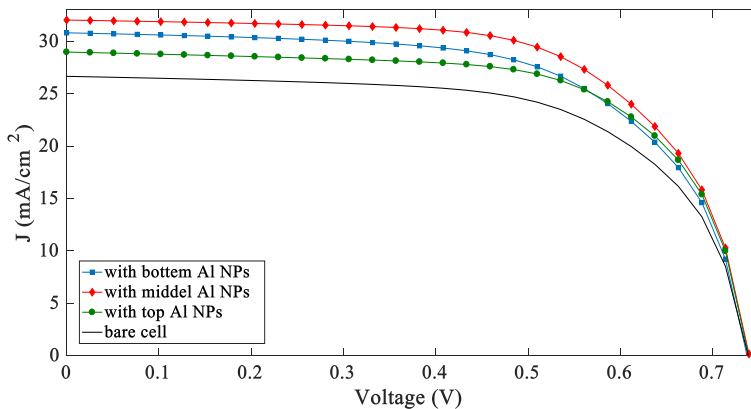


Fig. 7. J–V curve of ultrathin CIGS solar cells with three different locations of PNPs in comparison to the bare cell.

Table 2. Photovoltaic parameters of various ultrathin CIGS solar cells with three different locations of Al PNPs in comparison with the bare cell.

Vertical position	J _{sc} (mA/cm ²)	V _{oc} (V)	FF (%)	η (%)
Bare cell	26.65	0.735	64.19	12.57
Top	28.97	0.739	66.48	14.23
Middle	32.03	0.739	64.7	15.31
Bottom	30.8	0.739	62.79	14.29

4. Conclusion

In summary, a configuration including Al PNPs was proposed for an ultrathin CIGS solar cell to enhance light trapping. Decreasing CIGS thickness degraded the performance of the device. To improve the cell efficiency, using Al plasmonic nanoparticles was pursued. In first step, Al NPs were embedded at the top of the active layer, and the output parameters were calculated by FDTD method. Results showed a remarkable improvement of the performance of the ultrathin CIGS solar cell. It was also found that the enhancements in optical absorption and efficiency of the cell depends on the structural parameters (radius and period) of Al PNs array. All of these states were studied in details and the optimum results were achieved by carrying out the optical and electrical calculations. It was found that the current density and the efficiency of ultrathin CIGS solar cell can be increased considerably by using Al PNPs embedded in the middle of CIGS active layer.

REFERENCES

- [1] D. Jalalian, A. Ghadimi, A. Kiani Sarkaleh, *Investigation of the effect of band offset and mobility of organic/inorganic HTM layers on the performance of Perovskite solar cells*, J. Optoelectron. Nanostructures. 5(2) (2020) 65-78. Available: https://jopn.miau.ac.ir/article_4219.html
- [2] A. Abdolazadeh Ziabari, F. E. Ghodsi, *Growth, characterization and studying of sol-gel derived CdS nanocrystalline thin films incorporated in polyethyleneglycol: effects of post-heat treatment*, Sol. Energy Mater. Sol. Cells, 105 (2012) 249-262. Available: <https://doi.org/10.1016/j.solmat.2012.05.014>
- [3] K. Ahmadi, A. Abdolazadeh Ziabari, K. Mirabbaszadeh, S. Ahmadi, *Synthesis of TiO₂ nanotube array thin films and determination of the optical constants using transmittance data*, Superlattice Microst. 77 (2015) 25-34. Available: <https://doi.org/10.1016/j.spmi.2014.10.024>

- [4] Y. Sefidgar, H. Rasooli Saghai, H. G. Khiabani Azar, *Enhancing efficiency of two-band solar cells based on GaAs/InGaP*, 4(2) (2019) 83-102. Available: https://jopn.miau.ac.ir/article_3480.html
- [5] A. Abdolazadeh Ziabari, N. Mohabbati Zindanlou, J. Hassanzadeh, S. Golshahi, A. Bagheri Khatibani, *Fabrication and study of single-phase high-hole-mobility CZTS thin films for PV solar cell applications: influence of stabilizer and thickness*, J. Alloys Compd. 842 (2020) 155741. Available: <https://doi.org/10.1016/j.jallcom.2020.155741>
- [6] A. Abdolazadeh Ziabari, A. Bagheri Khatibani, *Optical properties and thermal stability of solar selective absorbers based on Co-Al₂O₃ cermets*, 55(3) (2017) 876-885. Available: <https://doi.org/10.1016/j.cjph.2017.02.015>
- [7] A. Abdolazadeh Ziabari, *Exploring low, moderate and heavy Al doping impacts on microstructure and optical attributes of nanostructured cadmium oxide thin films*, Superlattice Microst. 72 (2014) 172-185. Available: <https://doi.org/10.1016/j.spmi.2014.04.005>
- [8] A. Abdolazadeh Ziabari, A. H. Refahi Sheikhan, R. Vatani Nezafat, K. Monsef Haghighidoust, *Optical modeling and electrical properties of cadmium oxide nanofilms: developing a meta-heuristic calculation process model*, J. Appl. Phys. 117 (2015) 135303. Available: <https://doi.org/10.1063/1.4916720>
- [9] K. Ahmadi, A. Abdolazadeh Ziabari, K. Mirabbaszadeh, A. Ahadpour Shal, *Synthesis and characterization of ZnO/TiO₂ composite core/shell nanorod arrays by sol-gel method for organic solar cell applications*, Bul. Mat. Sci. 38 (2015) 617-623. Available: <https://doi.org/10.1007/s12034-015-0898-8>
- [10] M. A. Lahiji, A. Abdolazadeh Ziabari, *First-principle calculation of the elastic, band structure, electronic states, and optical properties of Cu-doped ZnS nanolayers*, Physica B Condens. Matter. 501 (2016) 146-152. Available: <https://doi.org/10.1016/j.physb.2016.08.033>
- [11] M. Nilkar, F. E. Ghodsi, A. Abdolazadeh Ziabari, *Compositional evolution and surface-related phenomena effects in ZnS-SiO₂ nanocomposite films*, Appl. Phys. A, 118 (2015) 1377-1386. Available: <https://doi.org/10.1007/s00339-014-8892-3>
- [12] A. Abdolazadeh Ziabari, S. M. Rozati, *Investigation of the effect of band-edge nonparabolicity on the carrier transport in ITO thin films*, 65 (2014) 487-490. Available: <https://doi.org/10.3938/jkps.65.487>

- [13] M. A. Lahiji, A. Abdolazadeh Ziabari, Ab-initio study of the electronic and optical traits of $\text{Na}_{0.5}\text{Bi}_{0.5}\text{TiO}_3$ nanostructured thin film, *J. Optoelectron. Nanostructures*. 4(2) (2019) 47-58. Available: https://jopn.miau.ac.ir/article_3474.html
- [14] M. Cheraghizade, Optoelectronic properties of PbS films: effect of carrier gas, *J. Optoelectron. Nanostructures*. 4(3) (2019) 47-58. Available: https://jopn.miau.ac.ir/article_3619.html
- [15] H. Izadneshan, G. Solookinejad, Effect of annealing on physical properties of $\text{Cu}_2\text{ZnSnS}_4$ (CZTS) thin films for solar cell applications, *J. Optoelectron. Nanostructures*. 3(2) (2018) 19-28. Available: https://jopn.miau.ac.ir/article_2861.html
- [16] Z. Dehghani Tafti, M. B. Zarandi, H. A. Bioki, Thermal annealing influence over optical properties of thermally evaporated SnS/CdS bilayer thin films, *J. Optoelectron. Nanostructures*. 4(1) (2019) 87-98. Available: https://jopn.miau.ac.ir/article_3387.html
- [17] R. Yahyazadeh, Z. Hashempour, Numerical modeling of electronic and electrical characteristics of 0.3 0.7 AlGaIn/GaN multiple quantum well solar cells, *J. Optoelectron. Nanostructures*. 5(3) (2020) 81-102. Available: https://jopn.miau.ac.ir/article_4406.html
- [18] M. Amiri, A. Eskandarian, A. Abdolazadeh Ziabari, *Performance enhancement of ultrathin graded $\text{Cu}(\text{InGa})\text{Se}_2$ solar cells through modification of the basic structure and adding antireflective layers*. *J. Photon. Energy* 10(2) (2020) 024504. Available: <https://doi.org/10.1117/1.JPE.10.024504>
- [19] S. Royanian, A. Abdolazadeh Ziabari, R. Yousefi, *Efficiency enhancement of ultra-thin CIGS solar cells using bandgap grading and embedding Au plasmonic nanoparticles*, *Plasmonics* 15 (2020) 1173–1182. Available: <https://doi.org/10.1007/s11468-020-01138-2>
- [20] E. Ghahremanirad, S. Olyaei, M. Hedayati, *The influence of embedded plasmonic nanostructures on the optical absorption of perovskite solar cells*, *Photonics* 6(2) (2019) 37. Available: <https://doi.org/10.3390/photonics6020037>
- [21] Lumerical Solutions, Inc. <http://www.lumerical.com/tcad-products/fdtd/>
- [22] Lumerical Solutions, Inc. <http://www.lumerical.com/tcadproducts/device/>
- [23] E.D. Palik, in *Handbook of Optical Constants of Solids*, ed. By E.D. Palik (Academic Press, New York, 1998).

- [24] W. Li, S. Xu, Y. Dai, P. Ma, Y. Feng, W. Li, H. Luo, C. Yang, *Improvement of the crystallinity and efficiency of wide-gap CIGS thin film solar cells with reduced thickness*, Mater. Lett. 244 (2019) 43–46. Available: <https://doi.org/10.1016/j.matlet.2019.02.031>
- [25] K. R. Catchpole, A. Polman, *Plasmonic solar cells*. Opt. Express 16 (26) (2008) 21793. <https://doi.org/10.1364/oe.16.021793>
- [26] M. Mirzaei, J. Hasanzadeh, A. Abdolazhadeh Ziabari, *Efficiency enhancement of CZTS solar cells using Al plasmonic nanoparticles: the effect of size and period of nanoparticles*, J. Electron. Mater. 49 (2020) 7168–7178. Available: <https://doi.org/10.1007/s11664-020-08524-w>
- [27] M. Amiri, A. Eskandarian, A. Abdolazhadeh Ziabari, *Performance improvement of ultra-thin CIGS solar cells with decrease in light loss by surface texturing*, Indian J. Phys. (2020). Available: <https://doi.org/10.1007/s12648-020-01888-z>
- [28] A. Mirkamali, K. K. Muminov, *Numerical Simulation of CdS/CIGS Tandem Multi-Junction Solar Cells with AMPS-1D*, J. Optoelectron. Nanostructures. 2(1) (2017) 31-40. Available: https://jopn.miau.ac.ir/article_2198.html
- [29] H. Izadneshan, V. Gremeno, G. Solookinejad, *Fabrication of Cu(In,Ga)Se₂ solar cells with In₂S₃ buffer layer by two stage process*, J. Optoelectron. Nanostructures. 1(2) (2016) 47-56. Available: https://jopn.miau.ac.ir/article_2048.html
- [30] S. M. S. Hashemi Nassab, M. Imanieh, A. Kamaly, *The effect of doping and thickness of the layers on CIGS solar cell efficiency*, J. Optoelectron. Nanostructures. 1(1) (2016) 9-24. Available: https://jopn.miau.ac.ir/article_1812.html

